PRE-PRINT of the article "Blocken B, Moonen P, Stathopoulos T, Carmeliet J. 2008. A numerical study on the existence of the Venturi-effect in passages between perpendicular buildings. **Journal of Engineering Mechanics – ASCE** 314(12).

A numerical study on the existence of the Venturi-effect in passages between perpendicular buildings

B. Blocken*[a], P. Moonen[b], T. Stathopoulos[c], F.ASCE, J. Carmeliet[d,e]

* Corresponding author

Abstract

The Venturi-effect refers to the increase in fluid speed due to a decrease of the flow section in confined flows. The wind speed conditions in converging and diverging passages between perpendicular buildings are studied with Computational Fluid Dynamics (CFD) to investigate the extent to which the so-called Venturi-effect is present in the passages. Model validation is performed by comparing the numerical results with wind tunnel measurements. The validated model is employed for a detailed investigation of the wind speed and the flow rate in the passages for a wide range of passage widths. The simulations show an increase in wind speed near ground-level but a decrease of horizontal wind speed in the upper part of the converging passages. The reason is the wind-blocking effect, which causes a large part of the oncoming wind to flow over and around the buildings, rather than being forced through the passage. Due to this effect, the flow rates through the converging passages are consistently lower than the free-field flow rate, implying that the term Venturi-effect is less applicable for such building configurations.

CE Database Subject Headings: Buildings; Computer aided simulation; Validation; Wind speed; Boundary layer flow; Fluid Dynamics; Turbulence; Acceleration; Pedestrians

[a] Assistant professor, Building Physics and Systems, Technische Universiteit Eindhoven, P.O. box 513, 5600 MB Eindhoven, The Netherlands, b.j.e.blocken@tue.nl, Tel. +31 40 247 2138, Fax +31 40 243 8595

[b] PhD student, Laboratory of Building Physics, Katholieke Universiteit Leuven, Kasteelpark Arenberg 40, 3001 Leuven, Belgium, peter.moonen@bwk.kuleuven.be

[c] Professor, Centre for Building Studies, Department of Building, Civil and Environmental Engineering, Concordia University, 1455 de Maisonneuve Blvd West, H3G 1M8, Montreal, Quebec, Canada, statho@bcee.concordia.ca

[d] Professor, Chair of Building Physics, Swiss Federal Institute of Technology ETHZ, ETH-Hönggerberg, CH-8093 Zürich, Switzerland

[e] Professor, Empa, Swiss Federal Laboratories for Materials Testing and Research, Laboratory for Building Technologies, Überlandstrasse 129, CH-8600 Dübendorf, Switzerland

1. Introduction

The Venturi-effect applies to confined flows and refers to the increase in fluid speed or flow rate due to a decrease of the flow section, where flow rate and flow cross-sectional area are inversely proportional (Venturi 1799). Because the increase in fluid speed is generally accompanied by a decrease in pressure (Bernoulli 1738), the term Venturi-effect is often also used to refer to Bernoulli's principle. Currently this terminology is being applied in the wider context of both confined and non-confined flows. The term "Venturi-effect" as pressure drop due to increase in speed, is generally used in e.g. medicine and in the automotive industry, whereas the same term is used in wind engineering/urban aerodynamics with the meaning of increase in speed due to flow constriction (e.g. Gandemer 1975; Lawson 1980; Dutt 1991).

Passages between buildings can be responsible for increased wind speed near ground-level that can cause wind nuisance for pedestrians (Wiren 1975; Gandemer 1975; Lawson 1980; Stathopoulos and Storms 1986; Stathopoulos and Wu 1995; To and Lam 1995; ASCE 2003; Blocken et al. 2007a). Wind conditions in passages also determine the extent of building interference effects (Huang and Gu 2005; Xie and Gu 2007). Several types of passages between buildings can be distinguished, including passages between parallel buildings placed side-by-side, passages between parallel shifted buildings and passages between perpendicular buildings. Depending on the wind direction, the passage in the latter category can be called a "converging passage" or a "diverging passage" (Fig. 1). The term Venturi-effect is typically associated with a converging passage, also called "Venturi-throat" (Gandemer 1975) (Fig. 1a). Most fundamental studies of wind conditions in passages between generic high-rise building configurations in the past have focused on passages between parallel buildings. Flow in passages between non-parallel high-rise buildings has received much less attention. Wiren (1975) performed wind tunnel measurements for perpendicular buildings, at pedestrian-level and for various wind directions (converging and diverging passages). Gandemer (1975) and Lawson (1980) only briefly reported wind tunnel results for converging passages. Beranek (1982) presented sand erosion tests for converging and diverging passages. Blocken et al. (2007b) performed wind tunnel measurements for perpendicular buildings as in Fig. 1, along the passage centerline at pedestrian-level, for various wind directions and for a wide range of passage widths.

A converging passage between buildings can be considered as a typical case of Venturi-effect. All studies mentioned above reported pedestrian-level amplification factors larger than unity in converging passages. The amplification factor K is defined as the ratio U/U_0, where U is the local wind speed and U_0 the reference wind speed (at the same location but without buildings present, i.e. the free-field wind speed). The different studies however seem to disagree on the physical process involved. While Gandemer (1975) and Lawson (1980) attributed the increased pedestrian-level wind speed in converging passages to the Venturi-effect, Wiren (1975) did not mention this effect, Beranek (1982) suggested it does not exist in converging passages between buildings, and Blocken et al. (2007b) mentioned the wind-blocking effect, rather than the Venturi-effect, as the most important physical process. The statements by these authors are briefly summarized and discussed below.

Gandemer (1975) mentions the following conditions for the occurrence of the Venturi-effect in a converging passage: (1) the minimum building height H has to be higher than 15 m; (2) the total length of the buildings ("Venturi arms") should not be less than 100 m; and (3) the surrounding environment should be free of any buildings over an area that is roughly equivalent to the one occupied by the building configuration. He also states that a maximum flow goes through the passage when the passage width w is 2 or 3 times the height H of the building. In that case, the comfort parameter ψ defined as

$$\psi = \frac{U + \sigma_u}{U_0 + \sigma_0} \quad (1)$$

would reach values up to 1.3 for building heights of 25 to 30 m and 1.6 for heights of about 50 m. All variables in Eq. 1 are taken at pedestrian height; U and σ_u are the local mean wind speed and the standard deviation of the turbulent fluctuations at the location of interest, and U_0 and σ_0 refer to the same quantities at the same location but without the buildings present (reference values). Stathopoulos and Storms (1986) demonstrated that the inclusion of wind gustiness (σ_u and σ_0) in the comfort parameter for passages between buildings makes little difference and that it can therefore be directly compared with the amplification factor U/U_0 that does not include turbulence. Lawson (1980) states that little acceleration occurs in the passage when the passage width is outside the interval [0.5H; 4H]. Unfortunately, Gandemer (1978) and Lawson (1980) did not report the test conditions and the details of their test results. As opposed to Gandemer (1975) and Lawson (1980), Beranek (1982) also provided data for diverging passages. His statement about the Venturi-effect was based on the observation that U/U_0 in diverging passages was systematically larger than in converging passages. Indeed, also Blocken et al. (2007b) found that U/U_0 in diverging

passages is often, but not always, larger than in converging passages. They hypothesized that these results might be explained by the wind-blocking effect rather than by the Venturi-effect. The wind-blocking effect refers to the slow-down of wind speed upstream of the buildings. This effect is more pronounced for the converging arrangements that "catch" the wind and significantly slow down a large mass of air over quite a large distance upstream of the passage ($r < 0$, see Fig. 1a). This will cause part of this air mass to flow around and over the passage, rather then being forced through the narrowest passage opening. It can explain why U/U_0 in converging passages is lower than in diverging passages.

At least part of the information available in the literature suggests that the increased pedestrian-level wind speed in a converging passage ("Venturi-throat") is caused by the Venturi-effect. This term is quite often used in relation to this type of passages. However, atmospheric flows around buildings are non-confined flows, and only part of the flow approaching a building group is expected to flow through the passage, while the rest will flow over and around the buildings. Therefore, it is not clear to what extent the Venturi-effect is really present and contributes to the increased amplification factors. In addition, previous studies of wind conditions in converging and diverging passages only focused on pedestrian-level wind speed, often along only one line in the passage. The information currently available in the literature about converging passages is very limited and does not allow clear conclusions to be made. A numerical study based on Computational Fluid Dynamics (CFD) can provide additional information for a more detailed investigation. A particular advantage of CFD is that it provides whole flow field data, whereas wind tunnel measurements are often point measurements. On the other hand, accurate wind tunnel measurements are important for CFD validation, which is an essential requirement before CFD can be used with confidence.

In this paper, CFD is employed for a detailed investigation of the wind speed conditions and the existence of the Venturi-effect in passages of converging-diverging building arrangements. First, model validation is performed by comparing numerical results with corresponding wind tunnel measurements. Next, the model is applied to calculate and analyze the wind speed and flow rate in the passages for a wide range of passage widths and the existence of the Venturi-effect is discussed. Finally, a general discussion and the conclusions are presented.

2. Model validation

2.1. Wind tunnel measurements

Measurements were conducted at a scale of 1:400 in the boundary layer wind tunnel of the Building Aerodynamics Laboratory at Concordia University (Stathopoulos 1984) and are reported in detail in (Blocken et al. 2007b). The basic building configuration and building dimensions are illustrated in Fig. 1, where r is a dimensionless coordinate along the passage centerline with $r = 0$ at the location of the narrowest passage opening. The unit length of r is $L\sqrt{2}/2$. The direction of the r-axis is according to the flow direction (positive in downstream direction). The building dimensions and experimental conditions were taken according to Gandemer's guidelines for the Venturi-effect (1975): $H = 30$ and 60 m (> 15 m), $2L = 200$ m (> 100 m) and open country exposure. Measurements were made for a range of passage widths. The measured incident mean wind speed profile (at $r = 0$; without buildings present) resembled a power-law function with exponent $\alpha = 0.125$. The reference incident wind speed U_0, taken at 5 mm height (pedestrian-level; 2 m in full scale) and at $r = 0$, was 7.4 m/s. The turbulence intensity of the incident flow, based on the local mean wind speed, ranged from 12% at 5 mm height to 2% at 0.75 m (300 m full scale). For all building configurations, the blockage ratio was lower than 1%. The building Reynolds number Re_b was 17,000. Mean wind speed and turbulence intensity measurements were made with a TSI hot-wire anemometer at pedestrian height at nine positions along the passage centerline: $r = -1, -0.5, -0.25, -0.125, 0, 0.125, 0.25, 0.5, 1$. The probe with a single-oriented hot wire was positioned so that the wire was horizontal and perpendicular to the passage centerline. Hot-wire measurements tend to overestimate the mean wind speed and underestimate the turbulent fluctuations in highly turbulent flows because of the well-known turbulence error (Cook and Redfearn 1976; Bottema 1993). The errors become more pronounced as turbulence intensity increases, and measurements are considered inaccurate when the turbulence intensity exceeds 30%. Because the present study mainly focuses on locations near $r = 0$, where mean wind speed is high and turbulence intensity is low, the measurements were considered suitable for model validation.

2.2. Numerical simulation

The experiments are reproduced by 3D CFD simulations with the commercial code Fluent 6.3.26. Simulations are made at a scale of 1:40, with the reference wind speed $U_0 = 7.4$ m/s as in the experiment. The reason for the adapted scale is to obtain suitable values for the dimensionless wall unit y^+ in the passages (between 30 and 100) to be able to use wall functions, without the need to change the reference wind speed or the grid resolution for this purpose. The dimensions of the computational domain are $L_D x B_D x H_D = 1400x1400x400$ m³ for $H = 30$ m and 1400x1400x800 m³ for $H = 60$ m (all full scale values).

A suitable grid is obtained based on grid-sensitivity analysis. Fig. 2(a) shows a top view of the grid at the bottom of the computational domain and Fig. 2(b) shows a detail of the grid on the building and ground surfaces near and in the passage. A structured hexahedral grid is used near the building surfaces (Fig. 2b) and near the outer boundaries of the domain (Fig. 2a). For grid economy, an unstructured grid with wedge cells (prisms) is used to bridge the region between the fine structured grid near the buildings and the coarse structured grid near the outer boundaries of the domain. The total number of cells is about 0.8×10^6.

Special attention is required concerning the boundary conditions, in particular the inlet mean wind speed and turbulence profiles and the implementation of the wall boundary condition. An important problem in many commercial CFD codes is the difficulty to simulate a horizontally homogeneous Atmospheric Boundary Layer (ABL) flow over uniformly rough terrain (Richards and Hoxey 1993; Blocken et al. 2007a, 2007c; Hargreaves and Wright 2007; Franke et al. 2007; Yang et al. 2007). Horizontal inhomogeneity (HIH) refers to the occurrence of streamwise gradients in the simulated vertical flow profiles as they flow through the upstream part of the computational domain, instead of the often requested equilibrium behavior. The reason is the inconsistency between inlet profiles, wall functions, ground roughness, grid and turbulence model (Blocken et al. 2007c). As a result the inlet profiles will generally differ from the profiles at the location in the domain where the buildings will be positioned ("incident-flow profiles"). This can have a detrimental influence on the accuracy of the simulation results and on validation studies (Blocken et al. 2007a). For Fluent 6, HIH can be limited by satisfying the required relationship between the aerodynamic roughness length y_0 of the inlet profiles and the input parameters k_S (equivalent sand-grain roughness height) and C_S (roughness constant) for the wall functions (Blocken et al. 2007c): $k_S = 9.793 y_0 / C_S$. This generally provides a very limited HIH for the mean wind speed profile, which is most important to accurately predict high wind speed amplification factors. However, turbulence profiles will generally show HIH to some extent. The streamwise gradients need to be assessed by a simulation in an empty computational domain.

The CFD inlet profiles are obtained from the wind tunnel incident profiles. The mean wind speed profile is the power law with $\alpha = 0.125$. Measured turbulence intensity I_u is converted to turbulent kinetic energy by assuming $\sigma_v = \sigma_w = \sigma_u/\sqrt{2}$: $k = \frac{1}{2}(\sigma_u^2 + \sigma_v^2 + \sigma_w^2) = \sigma_u^2 = (I_u U)^2$. Turbulence dissipation rate $\varepsilon = u^{*3}/\kappa(y+y_0)$, where y_0 and u^* are obtained by fitting a log law mean wind speed profile to the power law, yielding $y_0 = 0.00005$ m (value at CFD scale) and $u^* = 0.45$ m/s. The standard wall functions by Launder and Spalding (1974) with sand-grain roughness modification (Cebeci and Bradshaw 1977) are used. The requested relationship between y_0, k_S and C_S yields $k_S = 0.001$ m, $C_S = 0.5$ (all at CFD scale). At the outlet of the domain, zero static pressure is specified. The sides and the top of the domain are modeled as slip walls (zero normal velocity and zero normal gradients of all variables).

Steady-state 3D Reynolds-Averaged Navier-Stokes (RANS) simulations are made using the realizable k-ε model (Shih et al. 1995). Pressure-velocity coupling is taken care of by the SIMPLE algorithm. Pressure interpolation is second order. Second order discretization schemes are used for both convection terms and viscous terms of the governing equations. A simulation is made in an empty domain to assess the extent of horizontal homogeneity (HH) (Fig. 3). HH for the mean wind speed profile is very good, but the k-profile changes considerably when traveling through the domain.

Simulations are made for the converging and diverging arrangement, for w = 10, 30, 50, 60, 75, 90 m (H = 30 m) and for w = 10, 30, 50, 90 m (H = 60 m). For these passage widths, measurement results are available. CFD validation focuses on the amplification factors at pedestrian level along the passage centerline (K_{pcl}), at r = 0 (Fig. 1) and at the location where the measured K_{pcl} reaches its maximum value (r > 0). At these locations, the hot-wire measurements are accurate because of the low turbulence intensity ($I_u << 30\%$). A close agreement is obtained for all cases (Fig. 4), with better results for the maximum values, i.e. those important for design purposes. Note that a good agreement is obtained in spite of HIH of the k-profile.

3. Simulation results and analysis

Additional simulations, with the same boundary conditions and solver settings, are made for other passage widths, yielding results for w = 10, 15, 20, 30, 40, 50, 60, 75, 90 m for both H = 30 m and H = 60 m. The whole flow field results are analyzed in terms of the amplification factors K at pedestrian-level and in terms of flow rates (fluxes) through planes in and around the passages.

3.1. Analysis of pedestrian-level amplification factors

Fig. 5 displays contours of K in a horizontal plane at 2 m (full-scale) height above ground for a converging and a diverging building arrangement with H = 30 m and w = 75 and 20 m. The following observations are made:

(1) Fig. 5(a): Two separate corner streams with little interaction appear in the passage. The flow pattern around each building almost resembles the flow pattern around a single-standing building (separate corner streams,

stagnation region and wake). K is highest near the outer building corners, not in the passage. Also the region with high K-values is larger outside the passage.

(2) Fig. 5(b): The corner streams in the passage show a tendency to merge together into one wide passage jet, although the general flow patterns still show limited interaction. This is indicated by the fact that the highest K-values in the passage are not found in the center of the jet, but near the building corners in the passage.

(3) Comparing Figs. 5(a) and 5(b), it is clear that the pedestrian-level wind conditions are more severe in the diverging than in the converging passage. K-values in the diverging passage are larger but especially the area where high K-values are found is larger.

(4) Fig. 5(c): For w = 20 m, the separate corner streams in the passage can no longer be clearly distinguished and have merged into a single passage jet. High K-values are found in the jet and in the corner streams at the outer building corners. Similar to the wide passage, K is highest in these corner streams. A single large stagnation region is observed between the two buildings, and a single wake behind them, indicating that the buildings almost act as a single building. The stagnation region is very pronounced.

(5) Fig. 5(d): High K-values are found in the passage jet and in the corner streams. The values in the passage jet are larger than those in the corner streams.

(6) Comparing both figures, the pedestrian-level wind speed conditions are clearly more severe in the diverging passage.

The differences between the converging and diverging arrangements seem to support the statement that the wind-blocking effect governs the flow in the passages. Indeed, the slow-down of the upstream, streamwise horizontal wind speed due to the presence of the buildings is more pronounced for the converging arrangements. Fig. 5c clearly shows a large region of almost stagnant air between the two buildings. The oncoming wind that collides with this air mass will therefore rather be deviated over and around the buildings instead of being forced through the narrow passage opening. The wind-blocking effect is significantly less pronounced for the diverging arrangements, and therefore higher K-values are found here. Fig. 6 shows K_{pcl} (along the passage centerline) as a function of the co-ordinate r. The wind-blocking effect (r = -1 to r = 0) is clearly more pronounced for the converging arrangement. It also increases with decreasing passage width and increasing building height.

3.2. Analysis of fluxes and the Venturi-effect

The Venturi-effect refers to an average wind speed (or flow rate) in the passage rather than to wind speed at pedestrian level only. Therefore an analysis in terms of fluxes or flow rates is made based on the CFD results. Fig. 7 defines four fluxes: the horizontal flux of air F_P through the passage plane A_P, the horizontal flux F_H through the large vertical plane A_H, the vertical flux F_V through the horizontal plane A_V and the free flux F_F through a vertical plane A_F with the same size as the passage plane A_P but located outside the wind flow pattern that is disturbed by the buildings. The flux through a plane is calculated by integrating the velocity component normal to the plane over the area of the plane.

A converging building arrangement is a typical configuration for which the Venturi-effect could be present. In that case, one would expect F_P through the converging passage to be significantly larger than F_F. However, the simulation results yield the opposite conclusion: Fig. 8 shows that for the converging arrangements and for all passage widths investigated, F_P is smaller than F_F. Also, the ratio F_P/F_F for a diverging passage is systematically larger than for a converging passage.

The importance of the wind-blocking effect for the converging arrangements is indicated by the ratios F_V/F_H and F_P/F_H (Fig. 9). A significant amount of the air entering the passage plane A_H (F_H) does not exit through the passage plane A_P (F_P) but is deviated upwards and exits through the top plane A_V (F_V). For w = 10 m and H = 30 m, only 10% of the air entering the passage through A_H actually flows through the passage plane A_P. Even for the very wide passages (w = 90 m, H = 30 m), less than 50% of the air through A_H flows through A_P. The flow behavior for H = 60 m is very similar. The ratio F_P/F_H is slightly higher, because the higher building implies increased resistance for flow over the buildings.

It might seem contradictory that in the converging arrangements, the pedestrian-level wind speed is increased compared to free-field conditions ($K_{pcl,max} > 1$) while the passage flow rate is decreased compared to the free-field flow rate ($F_P/F_F < 1$). This difference is most pronounced for the narrowest passage, w = 10 m, where $K_{pcl,max}$ is highest and F_P/F_F is lowest. It can be explained by (1) the shape of the vertical mean wind speed profiles in the passage and (2) the location of the vena contracta beyond r = 0. Fig. 10 illustrates the amplification factor K_{pcp} (passage centerplane) along a vertical line at r = 0 for w = 10 m. K_{pcp} is defined as the ratio of the local, horizontal wind speed at a certain position (x,y,z) in the passage centerplane to the wind speed at the same position without the buildings present, i.e. the free-field reference wind speed at the same height. As a result, K_{pcp} is a direct indication of

the increase/decrease of the horizontal wind speed in the passage at all heights. The curves for the converging arrangements show strong vertical gradients, with a pronounced peak near ground-level and a strong decrease in the upper part of the passage. The peak is due to the downflow of air at the windward facades that subsequently flows through the passage near ground level (downflow, see Fig. 11). The downflow orginates from the deviation of the wind impinging on the facades. Part of this wind flow is deviated over the buildings, part flows along the facade in downstream direction and part is deviated towards the ground (Fig. 11). The decrease of K_{pcp} with height on the other hand is caused by the large amount of air that exits through the top plane A_V (upflow, see Fig. 11). The increase near ground-level is significantly more pronounced beyond r = 0 than at r = 0, due to the location of the vena contracta at r > 0 (Figs. 5c and 6). As shown in Fig. 6, $K_{pcl,max}$ indeed occurs beyond r = 0.

4. Discussion

The numerical simulations have provided information on the pedestrian-level wind conditions and on the air flow rates in the passages. The simulated amplification factors in diverging passages are generally higher than in converging passages, and their maximum values increase monotonically with decreasing passage width. This corresponds to the experiments by Wiren (1975), Beranek (1982) and Blocken et al. (2007b). However it does not correspond to the statements by Gandemer (1975) and Lawson (1980), because there is no maximum amplification factor in the passage for passage widths in the interval [2H; 3H] or in the interval [0.5H; 4H]. The numerical simulations have also shown that, at least for the building configurations studied here, there is no clear maximum in the passage flow rate F_P for passage widths in these intervals. Note that all building configurations studied were selected following the guidelines for the occurrence of the Venturi-effect (Gandemer 1975). In addition, the simulations have shown that for all passage widths investigated, the passage flux in a converging building arrangement is consistently lower than the free field flux.

The Venturi-effect has been defined as the increase in fluid speed or flow rate due to a decrease of the flow section. This terminology strictly only applies to flow in closed channels (Venturi 1799). For non-confined flows in wind engineering, the Venturi-effect could be defined in a similar way. Whether it can be stated that the Venturi-effect is present or not in a passage between buildings depends on the interpretation of this definition. In a very broad sense, the definition "the increase of wind speed due to a decrease of the flow section" can apply to any passage between buildings. Even a single-standing building on flat terrain will cause an increase of the wind speed somewhere at a location around its perimeter due to the decrease of the flow section by its presence. When the definition is interpreted more strictly, it should refer to an increase of the passage flux compared to the free-field flux. Following this definition, the Venturi-effect is not present for the converging arrangements studied in this paper. The reason is the wind-blocking effect, which causes the air to rather flow over and around the buildings than being forced through the narrow passage opening.

5. Conclusions

The wind speed conditions in converging and diverging passages between perpendicular buildings have been analyzed to determine the extent to which the Venturi-effect is present in the passages. The study found that at least for the building configurations (typical "Venturi"-cases) examined the following conclusions can be made:

1. For converging passages, there is an increase in wind speed near ground-level but a decrease of horizontal wind speed in the upper part of the passage. This is due to the wind-blocking effect, i.e. a large amount of the oncoming air flows over and around the buildings, rather than being forced through the passage opening. As a result, the wind flow rate through the converging passages is consistently lower than the free-field flow rate.
2. The Venturi-effect originally applied to flow in closed channels. This terminology cannot generally be extended to the non-confined flows in wind engineering. When the reference situation is a free-field situation, there is no increase in flow rate through the passages and strictly speaking, the so-defined Venturi-effect is not present.
3. Both pedestrian-level wind speed and air flow rates in the diverging passages are higher than in the converging passages, for which the wind-blocking effect is most pronounced.
4. More studies are needed to further expand the validity of the present findings.

Acknowledgements

Special thanks go to Sandra Johnson and her colleagues from the Niels Bohr Library of the American Institute of Physics, for their kind help to provide us with a copy of the old and precious text book by Giovanni Batista Venturi, translated by William Nicholson.

Notation

The following symbols are used in this paper:

Roman symbols

A	=	area (m²)
B, L, H	=	building width, length, height (m)
B_D, L_D, H_D	=	width, length, height of the computational domain (m)
C_S	=	roughness constant in the standard wall function modified-for-roughness (dimensionless)
F	=	flux or flow rate (kg/s or m³/s)
I_u	=	turbulence intensity (streamwise) (dimensionless)
K	=	amplification factor (dimensionless)
K_{pcl}	=	amplification factor along passage centerline (dimensionless)
K_{pcp}	=	amplification factor in the vertical passage centerplane (dimensionless)
k_S	=	physical roughness height (m)
U	=	horizontal component of the mean wind-velocity vector (m/s)
U_0	=	reference wind speed at pedestrian height (m/s)
U_g	=	gradient wind speed (m/s)
k	=	turbulent kinetic energy (m²/s²)
r	=	(relative) co-ordinate on r-axis (dimensionless)
Re_b	=	building Reynolds number (dimensionless)
u^*	=	friction velocity (m/s)
x, z	=	streamwise and spanwise co-ordinate (m)
y	=	height co-ordinate (m)
y_0	=	aerodynamic roughness length (m)
y^+	=	wall unit (dimensionless)

Greek symbols

α	=	power-law exponent (dimensionless)
ε	=	turbulence dissipation rate (m²/s³)
κ	=	von Karman constant (≈ 0.42)
$\sigma_u, \sigma_v, \sigma_w$	=	standard deviation of turbulent fluctuations in streamwise, vertical and lateral direction (m/s)
σ_0	=	reference value of σ (m/s)
ψ	=	comfort parameter (dimensionless)

References

ASCE (2003). Aerodynamics Committee. *Outdoor human comfort and its assessment*, State of the Art Report, Task Committee on Outdoor Human Comfort, American Society of Civil Engineers, Boston, VA, USA.

Beranek, W. J. (1982). *Beperken van windhinder om gebouwen*, deel 2, Stichting Bouwresearch no. 90, Kluwer Technische Boeken BV, Deventer, The Netherlands, 149 p + 89 p, (in Dutch).

Bernoulli, D. (1738). *Hydrodynamicae, sive de viribus et motibus fluidorum commentarii (Hydrodynamics, or commentaries on forces and motions of fluids)*, published Strasbourg, 1738. Translated from the Latin by T. Carmody and H. Kobus, published by Dover Publications, New York, 1972.

Blocken, B., Carmeliet, J., and Stathopoulos, T. (2007a). "CFD evaluation of wind speed conditions in passages between parallel buildings – effect of wall-function roughness modifications for the atmospheric boundary layer flow." *J. Wind Eng. Ind. Aerodyn.*, 95(9-11), 941-962.

Blocken, B., Carmeliet, J., and Stathopoulos, T. (2007b). "Wind environmental conditions in passages between two long narrow perpendicular buildings." *J. Aerospace Eng.*, Accepted for publication.

Blocken, B., Stathopoulos, T., and Carmeliet, J. (2007c). "CFD simulation of the atmospheric boundary layer: wall function problems." *Atmos. Environ.*, 41(2), 238-252.

Bottema, M. (1993). "Wind climate and urban geometry." PhD thesis. Building Physics Group, Technical University of Eindhoven, The Netherlands.

Cebeci, T. and Bradshaw, P. (1977). *Momentum transfer in boundary layers*. Hemisphere Publishing Corporation, New York.

Cook, N.J., and Redfearn, D. (1976). "Calibration and use of a hot-wire probe for highly turbulent and reversing flows." *J. Wind Eng. Ind. Aerodyn.*, 1(3): 221-231.

Dutt, A.J. (1991). "Wind flow in an urban environment." *Environ. Monit. Assess.*, 19(1-3), 495-506.

Franke, J., Hellsten, A., Schlünzen, H. and Carissimo, B. (2007). *Best practice guideline for the CFD simulation of flows in the urban environment*. COST Action 732: Quality Assurance and Improvement of Microscale Meteorological Models.

Gandemer, J. (1975). "Wind environment around buildings: aerodynamic concepts." *Proc., 4th Int. Conf. Wind Effects on Buildings and Structures*, Heathrow 1975, Cambridge University Press, 423-432.
Hargreaves, D.M., and Wright, N.G. (2007). "On the use of the k–ε model in commercial CFD software to model the neutral atmospheric boundary layer", *J. Wind Eng. Ind. Aerodyn.*, 95(5), 355-369.
Huang, P., and Gu, M. (2005). "Experimental study on wind-induced dynamic interference effects between two tall buildings". *Wind Struct.,* 8 (3): 147-161.
Launder, B.E., and Spalding, D.B. (1974). "The numerical computation of turbulent flows." *Comput. Method. Appl. M.,* 3, 269-289.
Lawson, T.V. (1980). *Wind effects on buildings, Vol. 1*, Applied Science Publishers Ltd., London, England.
Richards, P.J., and Hoxey, R.P. (1993). "Appropriate boundary conditions for computational wind engineering models using the k-ε turbulence model." Journal of *J. Wind Eng. Ind. Aerodyn.*, 46-47, 145-153.
Shih, T.H., Liou, W.W., Shabbir, A., and Zhu, J. (1995), "A new k-ε eddy-viscosity model for high Reynolds number turbulent flows – model development and validation." *Comp. Fluids,* 24(3), 227-238.
Stathopoulos, T. (1984). "Design and fabrication of a wind tunnel for building aerodynamics." *J. Wind Eng. Ind. Aerodyn.*, 16, 361-376.
Stathopoulos, T., and Storms, R. (1986). "Wind environmental conditions in passages between buildings." *J. Wind Eng. Ind. Aerodyn.*, 24, 19-31.
Stathopoulos, T., and Wu, H. (1995). "Generic models for pedestrian-level winds in built-up regions." *J. Wind Eng. Ind. Aerodyn.*, 54-55, 515-525.
To, A.P., and Lam, K. M. (1995). "Evaluation of pedestrian-level wind environment around a row of tall buildings using a quartile-level wind speed descriptor." *J. Wind Eng. Ind. Aerodyn.*, 54-55, 527-541.
Venturi, G.B. (1799). *Experimental enquiries concerning the principle of the lateral communication of motion in fluids: applied to the explanation of various hydraulic phenomena.* Translated from the French by Nicholson W, 1st English ed., J. Taylor, Architectural Library, High-Holborn, London.
Wiren, B.G. (1975). "A wind tunnel study of wind velocities in passages between and through buildings." *Proc., 4th Int. Conf. Wind Effects on Buildings and Structures*, Heathrow 1975, Cambridge University Press, 465-475.
Xie, Z.N., and Gu, M. (2007). "Simplified formulas for evaluation of wind-induced interference effects among three tall buildings." *J. Wind Eng. Ind. Aerodyn.*, 95 (1): 31-52.
Yang, W., Quan, Y., Jin, X., Tamura, Y., and Gu, M. (2007), "Influences of equilibrium atmosphere boundary layer and turbulence parameters on wind load distributions of low-rise buildings", *J. Wind Eng. Ind. Aerodyn.*, Accepted for publication.

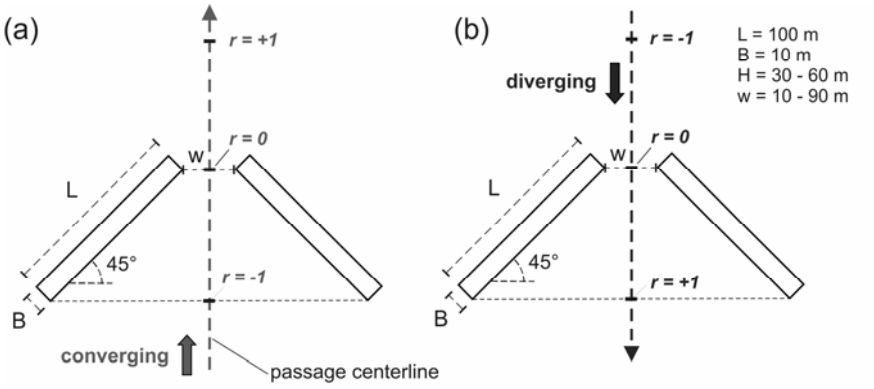

Fig. 1. Top view of (a) converging and (b) diverging passage between buildings, with indication of r-axis. The building dimensions mentioned are full-scale values.

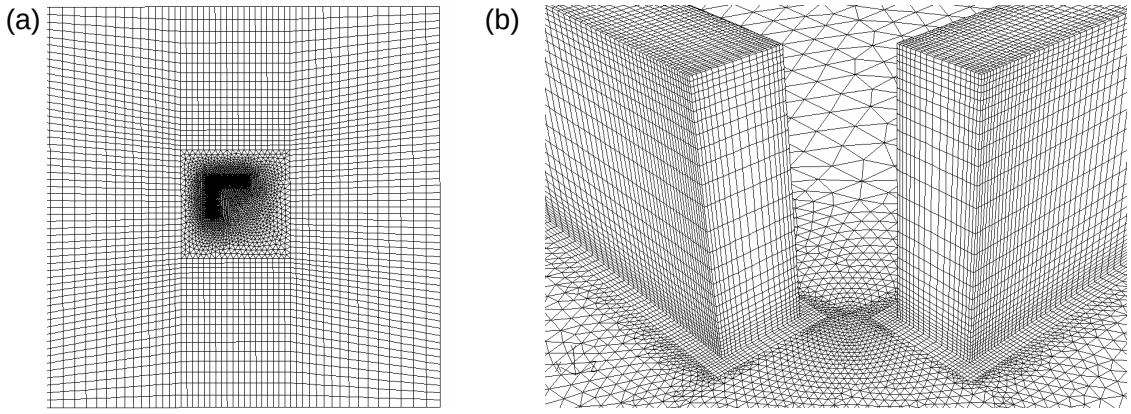

Fig. 2. (a) Top view of the grid at the bottom of the computational domain. (b) Perspective view of the grid at the building surfaces and at the ground surface near and in the passage.

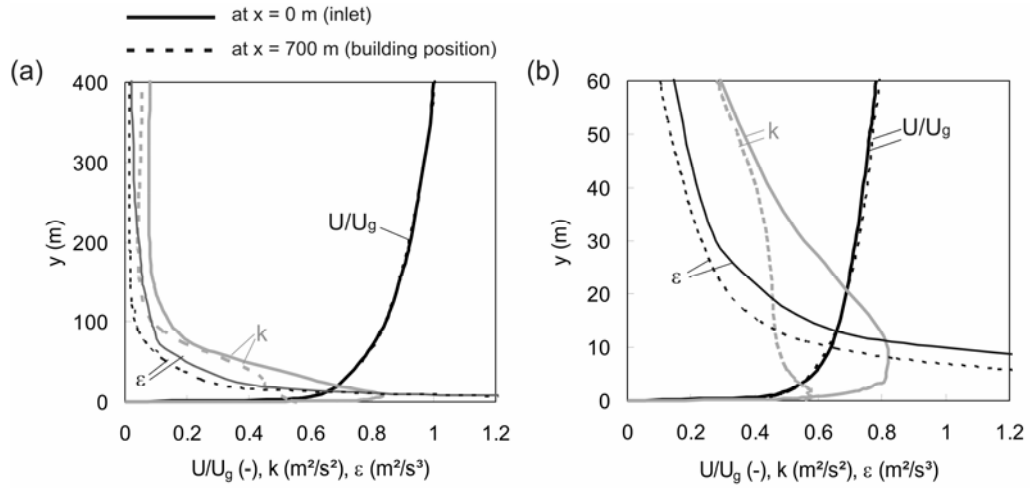

Fig. 3. Vertical profiles of ratio U/U_g, turbulent kinetic energy k and turbulence dissipation rate ε in an empty computational domain, at the inlet (approach flow) and where the buildings would be positioned (incident flow). (a) From 0 m to 400 m height, (b) From 0 m to 60 m height (= maximum building height).

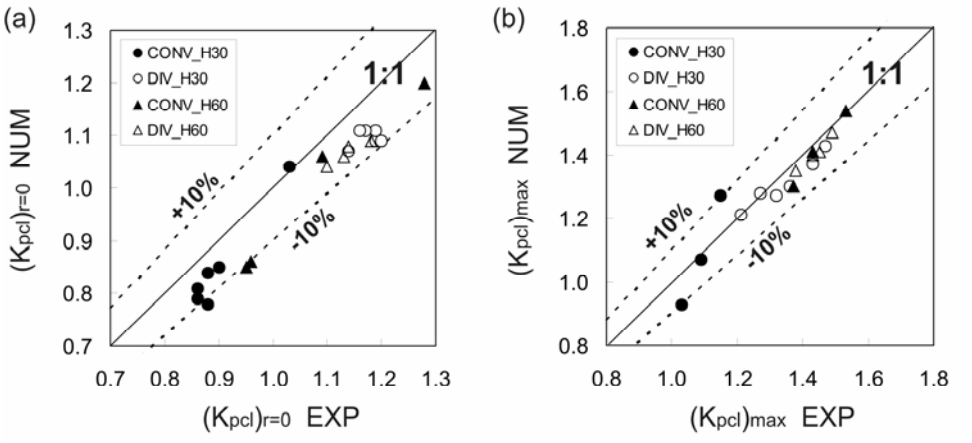

Fig. 4. Numerical versus experimental results for K_{pcl} for converging and diverging arrangement with H = 30 and 60 m. (a) K_{pcl} at r = 0. (b) K_{pcl} at position where its experimental value is maximum.

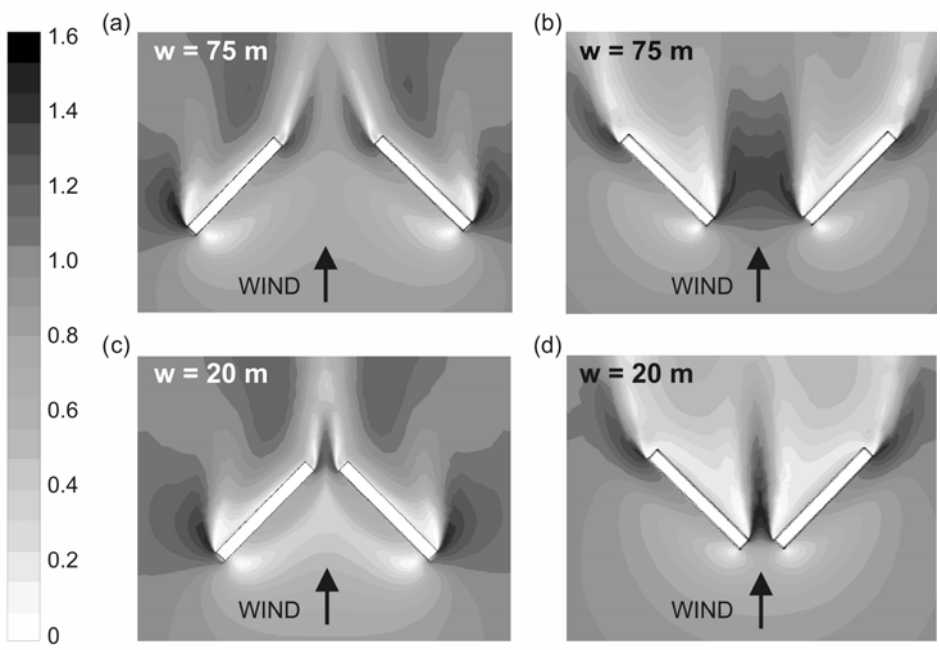

Fig. 5. Amplification factor K in a horizontal plane at y = 2 m (full scale) above ground for the converging and diverging arrangement with H = 30 m and for two passage widths.

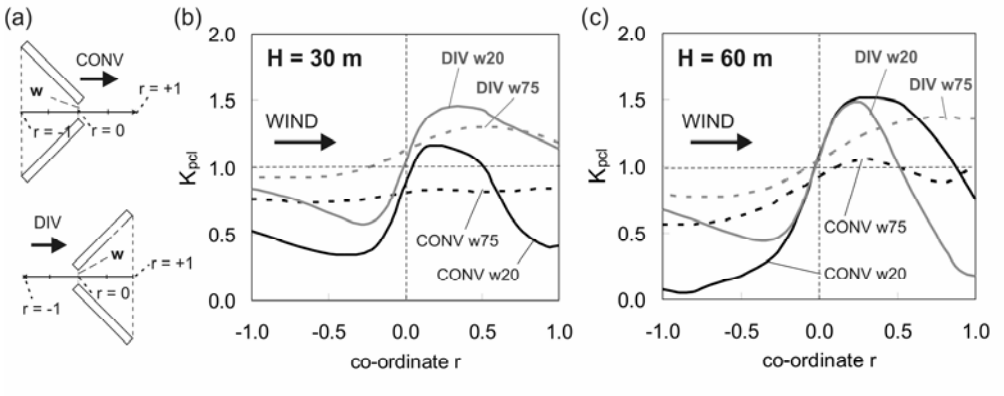

Fig. 6. (a) Schematic top view of converging (CONV) and diverging (DIV) flow and r-axis. (b) Amplification factor K_{pcl} along the passage centerline at 2 m height (full scale) for CONV and DIV with H = 30 m. (c) Same for H = 60 m.

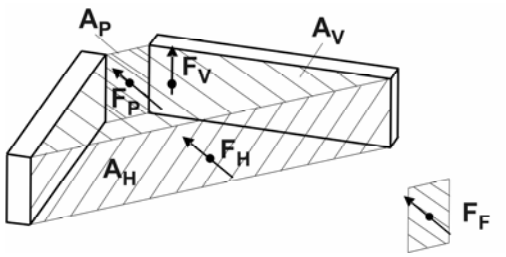

Fig. 7. Illustration and definition of areas and fluxes.

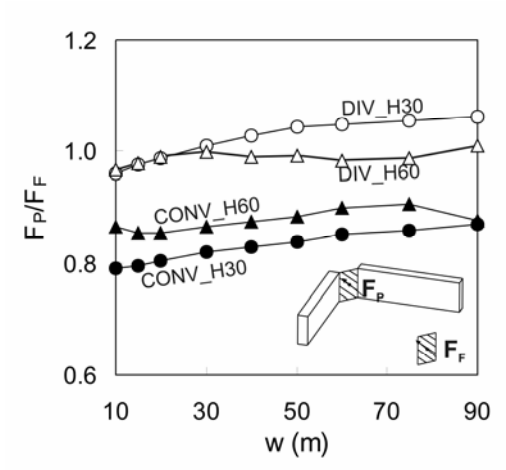

Fig. 8. Ratio of passage flux and free flux as a function of passage width, for converging and diverging arrangement and H = 30 and 60 m.

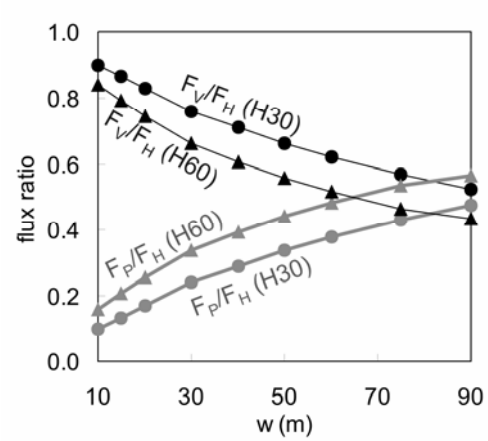

Fig. 9. Flux ratios F_V/F_H and F_P/F_H as a function of passage width, for the converging arrangement and H = 30 and 60 m.

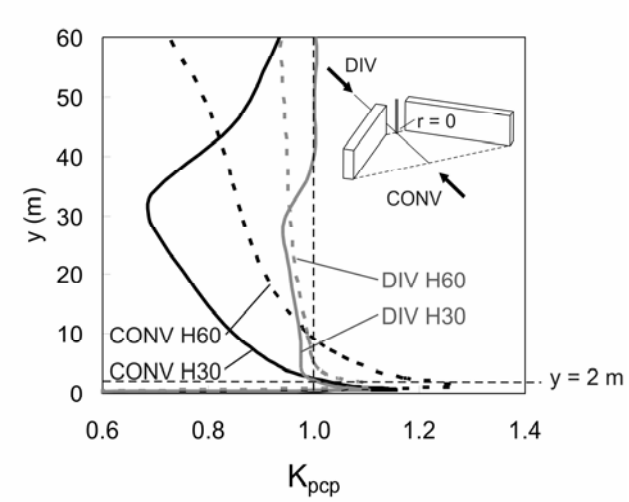

Fig. 10. Vertical profiles of amplification factor K_{pcp} at r = 0 for w = 10 m, for the converging and diverging arrangement and H = 30 and 60 m.

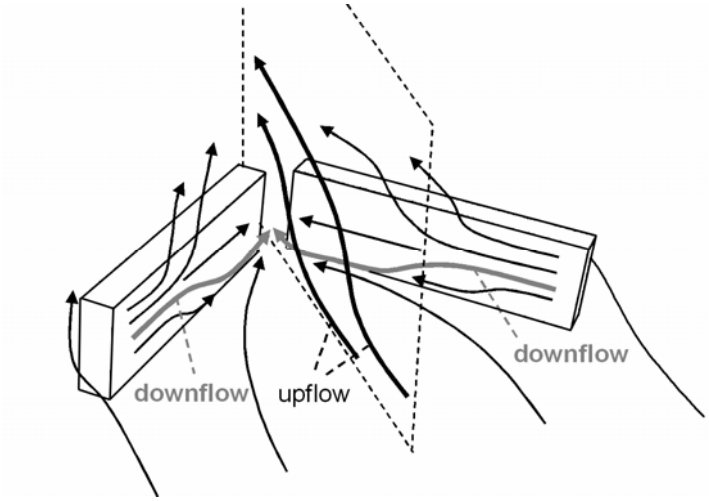

Fig. 11. Schematic representation of flow in the converging passage with H = 30 m and w = 10 m. The vertical plane cuts midway through the passage.

FIGURE CAPTIONS

Fig. 1. Top view of (a) converging and (b) diverging passage between buildings, with indication of r-axis. The building dimensions mentioned are full-scale values.
Fig. 2. (a) Top view of the grid at the bottom of the computational domain. (b) Perspective view of the grid at the building surfaces and at the ground surface near and in the passage.
Fig. 3. Vertical profiles of ratio U/U_g, turbulent kinetic energy k and turbulence dissipation rate ε in an empty computational domain, at the inlet (approach flow) and where the buildings would be positioned (incident flow). (a) From 0 m to 400 m height, (b) From 0 m to 60 m height (= maximum building height).
Fig. 4. Numerical versus experimental results for K_{pcl} for converging and diverging arrangement with H = 30 and 60 m. (a) K_{pcl} at r = 0. (b) K_{pcl} at position where its experimental value is maximum.
Fig. 5. Amplification factor K in a horizontal plane at y = 2 m (full scale) above ground for the converging and diverging arrangement with H = 30 m and for two passage widths.
Fig. 6. (a) Schematic top view of converging (CONV) and diverging (DIV) flow and r-axis. (b) Amplification factor K_{pcl} along the passage centerline at 2 m height (full scale) for CONV and DIV with H = 30 m. (c) Same for H = 60 m.
Fig. 7. Illustration and definition of areas and fluxes.
Fig. 8. Ratio of passage flux and free flux as a function of passage width, for converging and diverging arrangement and H = 30 and 60 m.
Fig. 9. Flux ratios F_V/F_H and F_P/F_H as a function of passage width, for the converging arrangement and H = 30 and 60 m.
Fig. 10. Vertical profiles of amplification factor K_{pcp} at r = 0 for w = 10 m, for the converging and diverging arrangement and H = 30 and 60 m.
Fig. 11. Schematic representation of flow in the converging passage with H = 30 m and w = 10 m. The vertical plane cuts midway through the passage.